TOPOLOGICAL AND GEOMETRICAL REASONING IN 3D GROUPING FOR RECONSTRUCTING POLYHEDRAL SURFACES

Stephan Heuel, Wolfgang Förstner[+] and Felicitas Lang[*]

[+] Institut für Photogrammetrie, Universität Bonn
Nussallee 15, D-53115 Bonn,
e-mail: Stephan.Heuel|Wolfgang.Foerstner@ipb.uni-bonn.de

[*] Institut für Photogrammetrie und Ingenieurvermessungen,
Universität Hannover
Nienburger Strasse 1, D - 30167 Hannover
email: felicitas.lang@ipi.uni-hannover.de

KEY WORDS: Building Extraction, 3D Grouping, Reasoning, Topology, Uncertain Geometry

ABSTRACT

We are developing a system for reconstructing polyhedral surfaces from multiple images. This process can take advantage of the topological relations of the observed image features triggering and therefore speeding up the grouping of features to polyhedral surfaces. Exploiting the statistical properties of features when grouping them leads to consistent decisions being invariant to numbering and choice of coordinate system and allows statistical testing. This simplifies the choice of thresholds to the definition of a scene independent significance level. We decribe the topological and statistical models used within our system. Experiments with synthetic and real data prove the feasibility of the approach.[†]

1 INTRODUCTION

Reconstructing polyhedral surfaces from multiple images is a classical task in Computer Vision. In case of controlled environment solutions are quite far advanced. However, in outdoor environments, e. g. when tracking vehicles or when reconstructing buildings, systems have to cope with quite a number of difficulties, such as a non-optimal feature extraction producing cluttered image descriptions with qualitative and quantitative errors. The technique of grouping significant features to high-level structures is often used to overcome some of these problems. The rules for grouping features are either very general and do not apply to real imagery or are rather specific and depend on the specific task. Most of the work was done in grouping two dimensional features but there also exists some work in 3D, for an overview see (Sarkar and Boyer, 1993).

Apart from early work (cf. (Clowes, 1971), (Brooks, 1987), (Herman and Kanade, 1986)), grouping straight lines or planes in 3D mostly appears in the context of building extraction from aerial images (cf. (Roux and McKeown, 1994), (Henricsson, 1996), (Frere et al., 1997) (Baillard et al., 1999)). These approaches, though embedded in a specific application appear to be the most general ones by restricting to polyhedral surfaces. The work of (Roux and McKeown, 1994) contains the most explicit use of 2D and 3D connectivity between features. (Baillard et al., 1999) generate plane hypothesis by half-plane detection and group 3D lines within these half-planes using collinearity and coplanarity criteria. Furtheron they close the half-planes by plane intersections.

All these systems primarily aim at finding at least *one path* from the basic features to object descriptions of generic nature and in this respect give valuable rules for grouping. However, due to the complexity of the objects and the need to use domain specific knowledge, no general grouping rules have been established.

We are developing a system for reconstructing polyhedral surfaces in outdoor environments aiming at exploiting as much generic knowledge as available from the structure of polyhedra, the imaging and the feature extraction process. There are two types of knowledge: a) neighborhood relations between the atomic features, points, edges and faces, resulting from *topology*, and b) crisp form relations at the object, especially planarity, and during the imaging process, resulting from *geometry*. On one hand, our feature extraction procedure (Förstner, 1994) was motivated by the need to exploit all features and their mutual neighborhood relations. In (Rothwell et al., 1996) topology as basic information in object representation

[†]This work has been founded by the European Community as part of the ESPRIT project "Image Processing for Automatic Cartographic Tools (IMPACT)", No. 20.243.

[*]This work originates from the time the author belonged to the Institute for Photogrammetry at the University of Bonn

was emphasized in the context of object recognition. On the other hand, crisp and qualitative geometry in reconstructing polyhedral scenes was the starting point for scene reconstruction (Clowes, 1971).

There are two basic problems to be tackled:
1. There appears to be no commonly accepted concept for topological relations in computer vision which can be used for reasoning. The setup in (Rothwell et al., 1996), though broard in scope, does not support the topological reasoning based on open sets.
2. The uncertainty of geometric entitites is a handicap for nearly all grouping systems, but needs to be conceptually embedded into the grouping processes. The difficulty is the aquisition and use of appropriate uncertainty measures as e. g. propagated by (Kanatani, 1995).

This paper adresses both problems: Its goal is to describe the topological and geometric concepts used in our system. As topological reasoning is computationally far superior to geometric reasoning, we try to always exploit topological knowledge before applying geometric checks. In order to minimize the number of control parameters for grouping the uncertainty of the geometric features is tracked through the system in a consistent manner using classical error propagation from 2D features to 3D structures. The feasability of this setup is demonstrated on real data, showing the usefulness of using topology and the advantage of exploiting the statistics of the geometric entities.

2 TOPOLOGY OF POLYHEDRA, THEIR IMAGES AND IMAGE FEATURES

2.1 Polyhedral Surfaces and their Images

Due to occlusions and the incompleteness of any feature extraction polyhedral objects can only be recovered partially from images. Without specific domain knowledge, e.g. restricting only the form of polyhedra, image analysis can reconstruct sets of *polyhedral surfaces*. Polyhedral surfaces are connected subregions of the surface of a polyhedron.

The structure of such surfaces is given by a set of well known constraints, inherited from polyhedra, especially concerning the neighbourhood relations between points P, edges E and regions R. These atomic elements are treated as open connected sets of dimension 0, 1 and 2 being the basis for topological neighborhood relations (Dold, 1972). The formal model is shown in fig. 1a.

If we first assume the faces of the polyhedron to have constant albedo and the illumination to be homogeneous, an ideal projection with infinite resolution leads to a Mondrian-type image, with points $\tilde{P}'$, edges $\tilde{E}'$ and region $\tilde{R}'$ showing relations with the same generic restrictions concerning the neighborhood relations. Occlusions yield missing features and missing and incorrect relations.

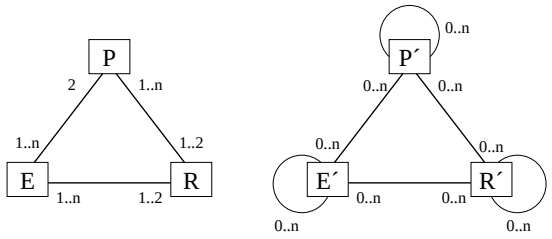

Figure 1: *a) shows the neighborhood relations between-points (P), edges (E) and regions (R) of a polyhedral surface. The multiplicity of the relations is constrained, given as range (e. g. $1..n$). The same generic constraints hold for the features $\tilde{P}'$, $\tilde{E}'$ and $\tilde{R}'$ of the ideal image. b) shows the possible relations between the observed image features P', E' and R' ($0..n$ means optional).*

2.2 Observable Image Features

We assume this ideal image is tried to be recovered with some feature extraction method. We use the method described in (Förstner, 1994, Fuchs, 1998) in general yielding points P', edges E', and regions R' which are assumed to have no overlap in the image plane. We also obtain neighborhood relations $N(F'_j, F'_k)$, directly by analysing the Voronoi diagram of all features F' (cf. fig. 6). There is no guarantee that all features or relations of the ideal projection can be detected. Much more, neighborhood relations may occur between features of the same type. This situation is depicted in fig. 1b, where no constraints on the number of neighborhoods can be found.

2.3 Relations between 3D Aggregates and their Generating Image Features

Starting from atomic features we may derive feature aggregates A in order to reach a higher level of aggregration. The rules for this aggregation process generally result from the image analysis task. The aggregation process can take advantage of the neighborhood relations. As we want to reconstruct polyhedral surfaces we are interested in basic 3D aggregates, namely point induced corners C, edge induced wings W and region induced meshes M as shown in fig. 2. These aggregates (A) may refer to the polyhedral surface representing local surface structures, to its ideal image ($\tilde{A}'$) triggering the grouping process or to the observed image (A') yielding a higher level of symbolic image description.

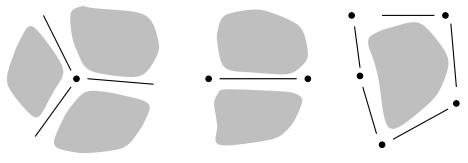

Figure 2: shows basic aggregates, corners, wings and meshes. Corners are most likely to show the same topology in the image (cf. (Clowes, 1971)).

Thus we obtain the following generic situation shown in fig. 3. Let the image features ${}^iF'$ and their neighborhood relations ${}^iN' \doteq N({}^iF'_j, {}^iF'_k)$ of image i be collected in the feature adjacency graph ${}^iFAG' = G({}^iF', {}^iN')$, being a compact representation of the situation in fig. 1b. Our goal is to reconstruct parts of the 3D *FAG* and to derive 3D aggregates together with their neighborhood relations, contained in the aggregate adjacency graph AAG. We want to discuss corners in detail, as they form the basis for our 3D recontruction procedure.

The 3D corners that are estimated in our approach are a special class of aggregates A. They are composed of 3D features F together with the used neighborhood relations. Fig. 3 represents the relation between the *FAG*'s in object resp. image space and the AAG.

The reconstruction starts at 3D-corners. Corners with $n \geq 1$ neighboring edges may be represented by $C^n = (P, E_1, \ldots, E_n, R_1, \ldots, R_m)$. The geometry of these 3D-features is given by the three coordinates of the corner point and the n directions of the edges.

Due to the multiple image redundancy the 3D edges $E_1, \ldots, E_2$ can be taken to be quite reliable. The generation of the 3D corners also establishes reliable neighborhood relations (incidences) between the 3D point and the 3D edges but also between the recovered 3D features F and the corresponding 2D features F'.

We also obtain neighboring planar regions $R_1, \ldots R_m$ with $\binom{n}{2} \geq m \geq 1$; but, without exploiting the 3D geometry in detail, e. g. by an occlusion analysis, they cannot be inferred reliably.

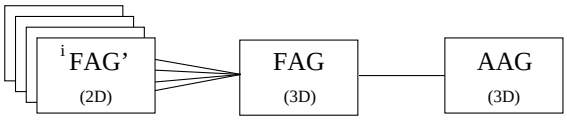

Figure 3: *Relationship of the graphs ${}^iFAG'$ of the images i, the 3D FAG and the graphs of the 3D aggregates, AAG. Some of these 2D features induce a set of 3D features and their neighborhood relationship, contained in the 3D FAG. Aggregating these features leads to entities like n-corners C^n, which in turn is part of the 3D AAG.*

The reconstruction process, descibed below (cf. 4.1), actually uses a set of image points and edges which, in a many-to-one relation, are linked to the 3D point and edges.

3 UNCERTAIN GEOMETRIC ENTITIES

Grouping 3D entities involves tests of various relationships between these entities. Geometric relationships play a central role, especially if they involve identities, incidences or other crisp conditions, as they can be used to either exclude merging processes with high reliability or to evaluate grouping results. Checking for the existence of these crisp relationships requires thresholds which depend on the uncertainty of the geometric parameters and therefore best are formulated as hypothesis tests. Thus we derived the uncertainty of the initially reconstructed 3D aggregates, especially corners, representing it in a covariance matrix and built a library for "statistical uncertain geometric reasoning", containing routines for generating 3D geometric entities and for checking geometric relations between them[1]. The concepts are similar to those of (Kanatani, 1995). Here we describe the process for generating uncertain 3D entities from image features and the basic elements of the geometric reasoning modules.

3D features are represented in two ways, an Euclidean one resulting from the reconstruction process and a homogeneous one for the spatial reasoning, which is used internally. The homogeneous representation, in contrast to using different maps, is continuous and allows also to represent entities at infinity. In all cases the uncertainty is represented by a covariance matrix of adequate rank, cf. (Förstner, 2000b).

We have to solve three tasks:
1. Transferring given entities into the internal representation.
2. Generating new entities from given ones.
3. Testing pairs of entities for specific geometric relations.

Table 1 summarizes the used representations.

entity	type	representation
$P(\mathbf{X})$	normal	$\boldsymbol{X}$
	hom.	$\mathbf{X} = (\boldsymbol{X}_0, X) \cong (\boldsymbol{X}, 1)$
$L(\mathbf{L})$	normal	$(\boldsymbol{X}, \boldsymbol{M})$
	hom.	$\mathbf{L} = (\boldsymbol{L}, \boldsymbol{L_0}) \cong (\boldsymbol{M}, \boldsymbol{X} \times \boldsymbol{M})$
$\varepsilon(\mathbf{A})$	normal	$(\boldsymbol{N}, D)$
	hom.	$\mathbf{A} = (\boldsymbol{A}, A_0) \cong (\boldsymbol{N}, D)$

Table 1: *shows the basic spatial entities with their different representation. The line parameters fullfill the condition $\boldsymbol{L} \cdot \boldsymbol{L}_0 = 0$. The vectors $\boldsymbol{M}$ and $\boldsymbol{N}$ represent normalized directions and normals resp.*

We realized modules for generating 3D entities from other given ones, namely, $L = P_1 \wedge P_2$, $L = \varepsilon_1 \cap \varepsilon_2$, $\varepsilon = P \wedge L$ and $P = L \cap \varepsilon$, where the operator $\wedge$ joins two entities, and the operator $\cap$ intersects two entities. A plane ε from three points $P_i, i = 1, .., 3$ is determined via $\varepsilon = (P_1 \wedge P_2) \wedge P_3$.

[1] This library `sugr`, written in C++ and in MAPLE is available upon request.

Table 2 collects the spatial relations which are useful for 3D-grouping. The explanation of the matrices $\mathbf{A}$ and $\mathbf{B}$ are given below. We now give an example for each of the three tasks.

Normalizing 3D points: 3D points are represented in homogeneous coordinates $\mathbf{X}$ with their length fixed, i. e. non-stochastic. Their 4×4 covariance matrix $\mathbf{\Sigma}_{XX}$ therefore has rank 3 and nullspace $\boldsymbol{h} = \mathbf{X}$. It is determined from the given 3×3 covariance matrix $\mathbf{\Sigma}'_{XX}$ of $\boldsymbol{X}$:

$$\mathbf{\Sigma}_{XX} = \boldsymbol{P}_h \begin{pmatrix} \mathbf{\Sigma}'_{XX} & \mathbf{0} \\ \mathbf{0}^\mathsf{T} & 0 \end{pmatrix} \boldsymbol{P}_h$$

using the projection matrix $\boldsymbol{P}_h = \boldsymbol{I} - \boldsymbol{h}(\boldsymbol{h}^\mathsf{T}\boldsymbol{h})^{-1}\boldsymbol{h}^\mathsf{T}$.

A line from 2 points: The line $L(\mathbf{L})$ through two points $P(\mathbf{X})$ and $Q(\mathbf{Y})$ is given by a 6-vector, its Plücker coordinates:

$$\begin{aligned} \mathbf{L} &= \begin{pmatrix} \boldsymbol{L} \\ \boldsymbol{L}_0 \end{pmatrix} = \begin{pmatrix} X\boldsymbol{Y}_0 - Y\boldsymbol{X}_0 \\ \boldsymbol{X}_0 \times \boldsymbol{Y}_0 \end{pmatrix} \\ &= \mathbf{A}(\mathbf{X})\,\mathbf{Y} = -\mathbf{A}(\mathbf{Y})\,\mathbf{X} \end{aligned}$$

with the 6×4 matrices

$$\mathbf{A}(\mathbf{X}) = \begin{pmatrix} X\boldsymbol{I} & -\boldsymbol{X}_0 \\ \boldsymbol{S}_{X_0} & 0 \end{pmatrix} \text{ and } \mathbf{A}(\mathbf{Y}) = \begin{pmatrix} Y\boldsymbol{I} & -\boldsymbol{Y}_0 \\ \boldsymbol{S}_{Y_0} & 0 \end{pmatrix}$$

with the matrix $\boldsymbol{S}_Y = [\boldsymbol{Y}]_\times$ inducing the cross product $\boldsymbol{Y} \times \boldsymbol{Z} = \boldsymbol{S}_y\boldsymbol{Z} = [\boldsymbol{Y}]_\times\boldsymbol{Z}$. Thus its covariance matrix $\mathbf{\Sigma}_{LL}$ of $\mathbf{L}(\mathbf{X}, \mathbf{Y})$ for correlated points $P(\mathbf{X})$ and $Q(\mathbf{Y})$ is given by:

$$\mathbf{\Sigma}_{LL} = (-\mathbf{A}(\mathbf{Y})\ \mathbf{A}(\mathbf{X})) \begin{pmatrix} \mathbf{\Sigma}_{XX} & \mathbf{\Sigma}_{XY} \\ \mathbf{\Sigma}_{YX} & \mathbf{\Sigma}_{YY} \end{pmatrix} \begin{pmatrix} -\mathbf{A}^\mathsf{T}(\mathbf{Y}) \\ \mathbf{A}^\mathsf{T}(\mathbf{X}) \end{pmatrix}$$

The covariance matrix has rank 4 with nullspace $\boldsymbol{H} = (\mathbf{L}, \overline{\mathbf{L}})$, where $\overline{\mathbf{L}}^\mathsf{T} = (\boldsymbol{L}_0{}^\mathsf{T}, -\boldsymbol{L}^\mathsf{T})$, the first column, due to the normalization to its length (cf. above), the second due to the orthogonality constraint between $\boldsymbol{L}$ and $\boldsymbol{L}_0$.

entities	relation	dof	test
P',P"	$P' \equiv P"$	3	$Y_i\mathbf{X} - X_i\mathbf{Y} = \mathbf{0}$
P, L	$P \in L$	2	$\mathbf{B}(\mathbf{L})\mathbf{X} = \mathbf{0}$
P, ε	$P \in \varepsilon$	1	$\mathbf{X}\cdot\mathbf{A} = \mathbf{0}$
L',L"	$L' \equiv L"$	4	$L''_i\mathbf{L}' - L'_i\mathbf{L}'' = \mathbf{0}$
	$L' \parallel L"$	2	$\boldsymbol{L}' \times \boldsymbol{L}'' = \mathbf{0}$
	$L' \cap L" \neq \emptyset$	1	$\mathbf{L}'\cdot\overline{\mathbf{L}}'' = \mathbf{0}$
	$L' \perp L"$	1	$\boldsymbol{L}'\cdot\boldsymbol{L}'' = 0$
L, ε	$L \in \varepsilon$	2	$\mathbf{B}(\overline{\mathbf{L}})\mathbf{A} = \mathbf{0}$
	$L \parallel \varepsilon$	2	$\boldsymbol{L} \times \boldsymbol{A} = \mathbf{0}$
	$L \perp \varepsilon$	1	$\boldsymbol{L}\cdot\boldsymbol{A} = 0$
ε', ε"	$\varepsilon' \equiv \varepsilon"$	3	$B_i\mathbf{A} - A_i\mathbf{B} = \mathbf{0}$
	$\varepsilon' \parallel \varepsilon"$	2	$\boldsymbol{A}' \times \boldsymbol{A}'' = \mathbf{0}$
	$\varepsilon' \perp \varepsilon"$	1	$\boldsymbol{A}'\cdot\boldsymbol{A}'' = 0$

Table 2: *shows 13 relationships between points, lines and planes useful for 3D grouping, together with the degree of freedom and the essential part of the test statistic. The index i in the condition $L' \equiv L"$is to be chosen such $|L_i, L''_i| >> 0$; analogously choose i for $P' \equiv P"$and $\varepsilon' \equiv \varepsilon"$. Observe, all tests are bilinear in the coordinates of the involved entities, thus allow rigorous error propagation.*

Testing the incidence of a point and a line: We want to test the relation $P(\mathbf{X}) \in L(\mathbf{L})$. Let us assume the line $L(\mathbf{L})$ is generated by two points $P_1(\mathbf{X_1})$ and $P_2(\mathbf{X_2})$. For an arbitrary point $Q(\mathbf{Y})$ the 4 points only are coplanar if the determinant $D = |\mathbf{X}\,\mathbf{X_1}\,\mathbf{X_2}\,\mathbf{Y}|$ vanishes. Using the Plücker-coordinates of $\mathbf{L^T} = (\boldsymbol{L}^\mathbf{T}, \boldsymbol{L}_\mathbf{0}^\mathbf{T})$ consisting of the six 2×2 determinants of $(\mathbf{X_1}\ \mathbf{X_2})$ we can write the determinant as the bilinear form, cf. (Weber, 1998), (Förstner, 2000a):

$$D = -\mathbf{X}^\mathsf{T}\mathbf{B}(\mathbf{L})\,\mathbf{Y} \doteq \mathbf{X}^\mathsf{T} \begin{pmatrix} -\boldsymbol{S}_L & \boldsymbol{L}_0 \\ \boldsymbol{L}_0{}^\mathsf{T} & 0 \end{pmatrix} \mathbf{Y} = \mathbf{Y}^\mathsf{T}\mathbf{B}(\mathbf{L})\mathbf{X} = \mathbf{Y}^\mathsf{T}\mathbf{A}^\mathsf{T}(\mathbf{X})\overline{\mathbf{L}}$$

This determinant vanishes for arbitrary points Q if $P \in L$, thus if the 4-vector[2]

$$\mathbf{D} \doteq -\mathbf{B}(\mathbf{L})\,\mathbf{X} = \mathbf{A}^\mathsf{T}(\mathbf{X})\,\overline{\mathbf{L}} = \mathbf{0}$$

is $\mathbf{0}$. The skew matrix $\mathbf{B}(\mathbf{L})$ has rank 2 and eigenvectors $(\boldsymbol{L}^\mathsf{T}, 0)$ and $((\boldsymbol{L} \times \boldsymbol{L}_0)^\mathsf{T}, |\boldsymbol{L}|^2)$. The hypothesis $\mathbf{D} = \mathbf{0}$ uses

$$T = \mathbf{D}^\mathsf{T}\mathbf{\Sigma}^+_{\mathbf{DD}}\mathbf{D} \sim \chi^2_\mathbf{2}$$

as test statistic which requires the pseudoinverse of the covariance matrix of $\mathbf{D}$. With the Jacobian $\boldsymbol{J} = \partial\mathbf{D}/\partial(\overline{\mathbf{L}}, \mathbf{X}) = (\mathbf{A}^\mathsf{T}(\mathbf{X}), -\mathbf{B}(\mathbf{L}))$ we obtain the covariancematrix of $\mathbf{D}$:

$$\mathbf{\Sigma}_{DD} = \mathbf{A}^\mathsf{T}(\mathbf{X})\mathbf{\Sigma}_{\overline{\mathbf{LL}}}\mathbf{A}(\mathbf{X}) + \mathbf{B}(\mathbf{L})\mathbf{\Sigma}_{\mathbf{XX}}\mathbf{B}(\mathbf{L})^\mathsf{T}$$

The covariance matrix $\mathbf{\Sigma}_{DD}$ has rank 2 and nullspace $\boldsymbol{H} = (\mathbf{X}, (\boldsymbol{L}^\mathsf{T}\ \mathbf{0})^\mathsf{T})$. This allows to determine the pseudo inverse from

$$\begin{pmatrix} \mathbf{\Sigma}^+_{DD} & * \\ * & * \end{pmatrix} = \begin{pmatrix} \mathbf{\Sigma}_{DD} & \boldsymbol{H} \\ \boldsymbol{H}^\mathsf{T} & \mathbf{0} \end{pmatrix}^{-1}$$

[2] $\mathbf{D} = \mathbf{B}(\mathbf{L})\,\mathbf{X}$ describes the plane passing through line $\mathbf{L}$ and point $\mathbf{X}$, which is undetermined if $P \in L$ or if $\mathbf{D} = \mathbf{0}$.

4.1 Generating 3D Corners

The corner reconstruction, cf. (Lang and Förstner, 1996), starts with selected image aggregates having the stuctural properties of 3D corners and thus probably being corners ${}^iC'$ in the i-th image. These image corners ${}^iC'$ are selected by point induced feature aggregation using the extracted features ${}^iF'$and their mutual neighborhood relations ${}^iN' \doteq N({}^iF'_j, {}^iF'_k)$ collected in the graph *FAG'*, cf. (Fuchs, 1998). Multi image correspondence analysis establishes an image corner correspondence evaluating the structural similarity of the image corners with respect to epipolar geometry. This correspondence set forms the basis for the transition to initially derived 3D corners C being corner hypotheses. These hypotheses have to be verified by multi image parameter estimation using all image features F' which support the hypotheses simultaneously. For verification the residuals of parameter estimation are used. Each n-corner C^n requires $3 + 2 \cdot n$ geometric parameters $\boldsymbol{g}$ being the three coordinates of the point vector $\boldsymbol{x}$ of the corner point P_0 and two parameters for each of the n edges E_k of the n-corner, being the direction angles α_k and the azimth β_k.

Besides the optimal estimates $\widehat{\boldsymbol{g}}$ of parameters the parameter estimation also gives their covariance matrix $\boldsymbol{\Sigma}_{\widehat{g}\widehat{g}}$, which is used to propagate the uncertainty of the corner reconstruction during 3D grouping. In order to have a link to the above mentioned geometric reasoning (sec. 3), we actually store the $n + 1$ 3D-points being the corner point P_0 and virtual points $P_n(\boldsymbol{X} + \boldsymbol{R}_k)$ along the corner edge direction which are given by the normalized direction vectors $\boldsymbol{R}_k = (\cos\alpha_k \cos\beta_k, \sin\alpha_k \cos\beta_k, \sin\beta_k)$,determined from the angle parameters α_k and β_k of the corner edge E_k. Starting with the covariance matrix $\boldsymbol{\Sigma}_{\widehat{g}\widehat{g}}$, one can easily derive the covariance matrix $\boldsymbol{\Sigma}_{xx}$ of the $n+1$ points by error propagation. Thus triplets of points are used for deriving corner planes $\varepsilon_m(\mathbf{A_m})$ (sec. 4.3) spanning the regions R_m including the corresponding covariance matrix $\boldsymbol{\Sigma}_{A_m A_m}$.

4.2 3D-Grouping

Now we want describe our approach to derive a description of polyhedral surfaces from the computed corners C^n derived in 4.1. The goal of the first two steps of the proposed grouping approach is to find those 3D entities, namely 2-corners and 1-corners (furtheron called directions), which belong to the same polyhedral surface. Starting from the set of n-corners $C^n = (P, E_1, \ldots, E_n, R_1, \ldots R_m)$ with $m = \binom{n}{2}$, we generate a set of m 2-corners $C^2 = (P, E_1, E_2, R(\varepsilon))$ for each n-corner C^n. Note that every 2-corner is neighbored to at least one region R which lie on a unique plane ε.

4.3 Grouping 2-corners of Surfaces

For grouping coplanar 2-corners we have to test $\binom{k}{2}$ pairs of corners $(C^2_{j'}, C^2_{j''})$, where k is the total number of 2-corners. If we would only apply a geometrical test on coplanarity, we might group corners, which actually refer to *different* polyhedral surfaces but are accidentally planar (see example 5). Furthermore, solely testing coplanarity can be quite time consuming, depending on k and the time-behaviour of the geometrical test. Therefore we first exploit the topology of the underlying images i, namely the relations of the *FAG'*, cf. 2.3, before applying a geometrical test. Using topology is most likely not as time-consuming as using geometry, since it is only a look-up on the known data.

Selecting Hypotheses using Topology: Here we apply the analysis of relations of 2D and 3D features and aggregates as described in 2.3. A pair of corners (C^2_1, C^2_2) belongs to the same mesh (i.e. a 3D polyhedral surface including its boundary, cf. 2.1) if they are both neighbored to the same 3D-region, i. e. they are related in the AAG. This relation in 3D also can possibly be found in the relations of the *FAG'* of the images. We can use this fact to select those pairs of corners satisfying the following condition: suppose $\mathcal{E}'_1$ resp. $\mathcal{E}'_2$ to be the set of image edges inducing the corners C^2_1 resp. C^2_2. These image edges again are neighbored to a set of image regions $\mathcal{R}'_1$ resp. $\mathcal{R}'_2$ of all images. If the intersection $\mathcal{R}'_1 \cap \mathcal{R}'_2$ is not empty, we can infer the hypothesis that the 3D-edges of the corners C^2_1, C^2_2 share at least one 3D-region.

Testing Hypothesis using Geometry: We now take the selected pairs of corners from 4.3 and group them with respect to coplanarity. Since the two corners are statistically uncertain, we apply the method described in sec. 3: we compute the plane ε_1 resp. ε_2 of the 2-corners C^2_1 resp. C^2_2 and their covariance matrices $\boldsymbol{\Sigma}_{A_1A_1}$ resp. $\boldsymbol{\Sigma}_{A_2A_2}$ and test the condition $\varepsilon_1 \equiv \varepsilon_2$. If this is true, we assume that the two 2-corners belong to the same polyhedral surface. Testing this for all selected cornerpairs, we obtain a number of grouped sets $\mathcal{G} = \{G_g\} = \{\bigcup C^2_{gj}\}$ of 2-corners, which are identified to belong to the same surface.

4.4 Grouping Directions of Surfaces

A direction is a 1-corner $D := C^1 = (P, E)$, generated from an n-corner, similar to 4.3. In this step we want to include those directions, which belong to the surface, but have not been covered by the above grouping process. This is possible as one can see in fig. 4. To find those directions D, we again first apply a selection based on topology before geometrically testing planarity.

Selecting Hypotheses using Topology: We consider all possible pairs (G, D) of grouped sets G from 4.3 and directions D. With the same argument as in 4.3, we can compare the neighbored 2D-regions $\mathcal{R}'_1$ of G with the neighbored 2D-regions $\mathcal{R}'_2$ of the direction D. If the intersection of these 2D-region sets is not empty, we accept this pair for the subsequent geometrical test.

Testing Hypothesis using Geometry: From the grouped set of corners G we can compute an averaged plane $\varepsilon(\overline{\mathbf{A}})_G$ with an averaged covariance matrix $\mathbf{\Sigma}_{\overline{AA}}$. From the direction D we can compute a line L with $\mathbf{\Sigma}_{LL}$. If the geometrical test does not reject $L \in \overline{\varepsilon}_G$, we include D to the grouped set of corners G.

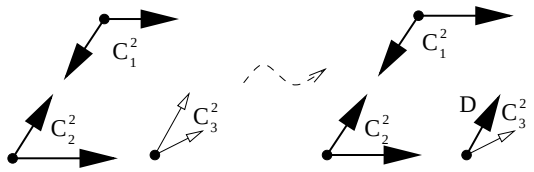

Figure 4: *The 2-corners C_1^2 and C_2^2 are coplanar, but not with C_3^2. One direction $D \in C_3^2$ is coplanar to C_1^2 and C_2^2. Black arrows indicate directions within a group.*

4.5 Grouping Directions to 3D Edges

At this stage of grouping we know, which corners and directions belong to the same surface. Now the task is to connect the corners C^2 and directions $D := C^1$ so that the connections are (estimated) 3D edges of the polyhedral surface.

Selecting Hypotheses using Topology: Each direction $D \in C^2$ of a corner C^2 resp. a direction D from 4.3 refers to a set $\mathcal{E}'(D)$ of 2D image edges. Again, using the analysis of relations of 2D and 3D features and aggregates in 2.3, a pair of directions (D_1, D_2) belongs to the same 3D edge if they share at least one 2D edge, i.e. $\mathcal{E}'(D_1) \cap \mathcal{E}'(D_2) \neq \emptyset$. Note that we do not test all directions in the scene, but only those belonging to the same grouped set G of corners.

Testing Hypotheses using Geometry: It is still possible that the topology selection above results in pairs (D_1, D_2) of 3D-direction, which are not collinear to each other, e.g. when having an accidental view. Therefore we test the two lines L_1, L_2 with $\mathbf{\Sigma}_{LL}$ induced by the directions: $L_1 \equiv L_2$. If a pair of direction also succeeds this test, we assume to have a polyhedral edge between them.

4.6 Generating 2-Corners from 3D Edges

The step described in 4.5 may already result in a complete boundary description of a polyhedral surface. This boundary description can be interpreted as an undirected graph. Then the boundary is called complete if the graph consists of one cycle. However, if there is no cycle in the graph, we might be able to add a vertex and replace two graph-edges in order to get a cycle. An addition of a vertex is the same as estimating a new 2-corner on the surface; replacing two edges is the same as grouping the two directions of the new 2-corner to two new 3D-edges of the surface. We can do this by computing the intersection of direction pairs (D_1, D_2), where the directions D_i refer to vertices of arity 1. We only consider those intersections which lie on the directions; its projection in the images must be within the image bounds. If there is more than one possible intersection for one direction, we take the one closest to vertex of arity 1.

4.7 Generating 3D Edges from 2D Edges

Now we still might have an incomplete boundary of the surface, e.g. a U-shaped boundary, where two directions are parallel to each other. We do not have 3D information to fill the gap at this stage of the analysis, we'd have to go back to the images and project appropriate 2D edges (selected by an anlaysis of the ${}^iFAG'$) to the planar surface. The we have to find the intersections of the projedted 2D edge with the parallel direction. This has currently not been implemented yet. As a first guess we just close a U-shape boundary by connecting the vertices of arity 1.

5 RESULTS

We have tested our grouping approach described in sec. 4 on one synthetic scene with two polyhedra (cf. fig 5) and with 11 aerial scenes containing one building each (cf. figs. 6 and 7) without changing any parameters. Alltogether 110 n-corners have been generated, containing 232 directions.

We excluded those directions where the averaged standard deviation $\sigma_{\overline{\alpha,\beta}} := \sqrt{\frac{\sigma_\alpha^2 + \sigma_\beta^2}{2}}$ of the direction angles α and β exceeded 10°, thus rejecting bad observations. The algorithm found 62 polyhedral surfaces. Table 3 documents the effect of topological selection prior the geometrical test, the reduction rate in the three grouping stages in sec. 4.3–4.5 is less than 40%. It can also be seen that the topological test on shared 2D lines sec. 4.5 is more reliable than the ones of intersecting 2D regions in 4.3 resp. 4.4, cf. third column.

6 CONCLUSIONS

This paper presents a procedure for 3D grouping by combination of topological and geometrical reasoning. It shows the advantage of using topological reasoning to efficiently reduce the number of geometric checks to be performed while feature grouping. The topological reasoning is based on a close interaction of 2D and 3D information to exploit the redundancy of the observed FAG's in image space. While subsequently checking geometrical relations we use rigorous statistical testing which allowed to use the same control parameters for all examples and thus supports the generality of the approach. the experiments with real data demonstrated the feasibility of the approach. Future work is directed toward integrating single points, but more important, lines or wings ((Baillard et al., 1999)) and possibly regions or meshes in order to improve completeness of the reconstructions. We also will investigate the impact of integrating range data, either from stereo or from laser scanners, (Brunn, 2000). [3]

REFERENCES

Baillard, C., Schmid, C., Zisserman, A. and Fitzgibbon, A., 1999. Automatic line matching and 3d reconstruction of buildings from multiple views. In: ISPRSGIS99, pp. 69–80.

Brooks, R., 1987. Model-based three-dimensional interpretation of two-dimensional images. In: M. Fischler and O. Firschein (eds), Readings in Computer Vision, Morgan Kaufmann, pp. 360–370.

Brunn, A., 2000. A step towards semantic-based building reconstuction using markov-random-fields. In: Proceedings of the XIXth ISPRS Congress, Vol. XXXIII, Part B, ISPRS, Amsterdam.

Clowes, M., 1971. On seeing things. Artificial Intelligence 2, pp. 79–116.

Dold, A., 1972. Lectures on Algebraic Topology. Springer, Berlin.

Förstner, W., 1994. A Framework for Low Level Feature Extraction. In: J. O. Eklundh (ed.), Computer Vision - ECCV 94, Vol. II, LNCS, Vol. 802, Springer, pp. 383–394.

Förstner, W., 2000a. New orientation procedures. In: Proceedings of the XIXth ISPRS Congress, Vol. XXXIII, ISPRS, Amsterdam.

Förstner, W., 2000b. Repräsentation und Prüfung von Beziehungen unsicherer geometrischer Elemente im Raum. In: J. Albertz (ed.), Photogrammetrie und Fernerkundung – Neue Sensoren/Neue Anwendungen, Vol. 8, DGPF, Berlin.

Frere, D., Hendrickx, M., Vandekerckhove, J., Moons, T. and van Gool, L. ., 1997. On the reconstruction of urban house roofs from aerial images. In: G. A., E. Baltsavias and O. Henricsson (eds), Automatic Extraction of Man-Made Objects from Aerial and Space Images (II), pp. 87–96.

Fuchs, C., 1998. Extraktion polymorpher Bildstrukturen und ihre topologische und geometrische Gruppierung. DGK, Bayer. Akademie der Wissenschaften, Reihe C, Heft 502.

Henricsson, O., 1996. Analysis of Image Structures using Color Attributes and Similarity Relations. PhD thesis, Swiss Federal Institute of Technology, ETH Zürich, No. 11663.

Herman, M. and Kanade, T., 1986. The 3d mosaic scene understanding system. In: A. Pentland (ed.), From Pixels to Predicates, Norwood N.J. Ablex Publ. Co.

Kanatani, K., 1995. Statistical Optimization for Geometric Computation: Theory and Practice. 2 edn, AI Laboratory, Gunma University, Japan.

Lang, F. and Förstner, W., 1996. Surface reconstruction of man-made objects using polymorphic mid-level features and generic scene knowledge. Zeitschrift für Photogrammetrie und Fernerkundung 6, pp. 193–201.

Rothwell, C., Mundy, J. and Hoffman, B., 1996. Representing objects using topology. In: J. Ponce, A. Zisserman and M. Hebert (eds), ECCV '96, International Workshop, Lecture Notes in Computer Science, Springer-Verlag, pp. 80–108.

Roux, M. and McKeown, D. M., 1994. Feature matching for building extraction from multiple views. In: ARPA IU Workshop '94, Vol. I, Monterey, California, Morgan Kaufman, ISBN 1-55860-338-7. 13-16 Nov.

Sarkar, S. and Boyer, K., 1993. Perceptual organization in computer vision: A review and a proposal for a classificatory structure. Transaction on Systems, Man, and Cybernetics 23, pp. 382–399.

Weber, M., 1998. Quadrik Through three Lines. personal communication, Bonn.

[3] Acknowledgements: The authors would like to thank Thomas H. Kolbe and Markus Zink for providing parts of the implementation.

Grouping Stage	All Tests	Topology Selection		Geometrical Approval	
sec. 4.3	1007	361	(36%)	98	(27%)
sec. 4.4	1363	362	(27%)	219	(60%)
sec. 4.5	328	73	(22%)	53	(72%)

Table 3: *The table lists statistics for the three grouping stages desribed in sec. 4.3–4.5. The first column lists the number of all possible tests at this stage. The second column gives the number of selected tests just by using topology, additionally the reduction factor is given in percentage. The third column contains the number of succesful geometrical tests; here, the number in brackets gives the percentage of accepted geometrical tests from the accepted topology tests—if it would equal 100%, the geometric test would be useless.*

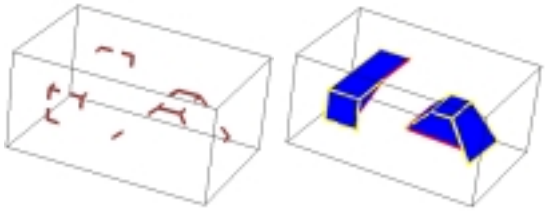

Figure 5: *Synthetic example. The left picture shows the set of generated n-corners and the right the set of reconstructed surfaces from these corners. Note that the top surfaces of the two polyhedra are detected as distinct though coplanar.*

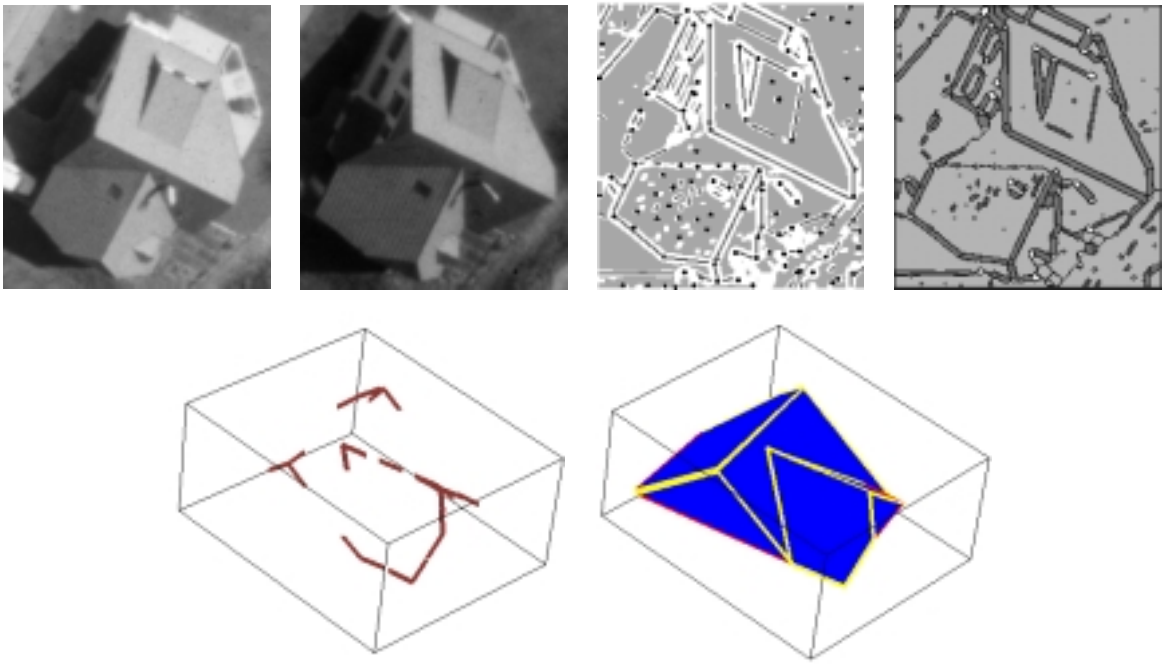

Figure 6: *Building example 1. The first row shows two out of four images for one tested aerial scene , the feature extraction for one image and the Voronoi diagram of the features yielding to neighborhood relations of features (cf. sec.2.1). The second row shows the set of generated n-corners (left) and the set of reconstructed surfaces (right).*

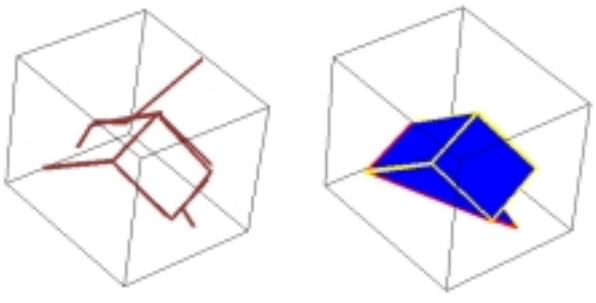

Figure 7: *Building example 2. Another reconstruction of an aerial scene with a set of n-corners (left) and the found surfaces (right). Note that the long direction in the back of the scene was removed because of the bad standard deviation of the angles.*